ELSEVIER

Real-time nanoscale observation of deformation mechanisms in CrCoNi-based medium- to high-entropy alloys at cryogenic temperatures

Qingqing Ding [1], Xiaoqian Fu [1], Dengke Chen [2], Hongbin Bei [3], Bernd Gludovatz [4], Jixue Li [1], Ze Zhang [1], Easo P. George [3,5], Qian Yu [1,*], Ting Zhu [2,*], Robert O. Ritchie [6,7,*]

[1] Department of Materials Science & Engineering, Center of Electron Microscopy and State Key Laboratory of Silicon Materials, Zhejiang University, Hangzhou 310027, China
[2] Woodruff School of Mechanical Engineering, Georgia Institute of Technology, Atlanta, GA 30332, USA
[3] Materials Science and Technology Division, Oak Ridge National Laboratory, Oak Ridge, TN 37831, USA
[4] School of Mechanical and Manufacturing Engineering, UNSW Sydney, NSW 2052, Australia
[5] Materials Science and Engineering Department, University of Tennessee, Knoxville, TN 37996, USA
[6] Materials Sciences Division, Lawrence Berkeley National Laboratory, Berkeley, CA 94720, USA
[7] Department of Materials Science & Engineering, University of California, Berkeley, CA 94720, USA

Technologically important mechanical properties of engineering materials often degrade at low temperatures. One class of materials that defy this trend are CrCoNi-based medium- and high-entropy alloys, as they display enhanced strength, ductility, and toughness with decreasing temperature. Here we show, using *in situ* straining in the transmission electron microscope at 93 K (−180 °C) that their exceptional damage tolerance involves a synergy of deformation mechanisms, including twinning, glide of partials and full dislocations, extensive cross-slip, and multiple slip activated by dislocation and grain-boundary interactions. In particular, massive cross-slip occurs at the early stages of plastic deformation, thereby promoting multiple slip and dislocation interactions. These results indicate that the reduced intensity of thermal activation of defects at low temperatures and the required increase of applied stress for continued plastic flow, together with high lattice resistance, play a pivotal role in promoting the concurrent operation of multiple deformation mechanisms, which collectively enable the outstanding mechanical properties of these alloys.

Introduction

Metallic materials can be exposed to extremely low temperatures in certain service environments, such as those experienced by fuel tanks, pressure vessels, pipelines in cold regions, structures for fusion power, hydrocarbon exploration, and certain aerospace applications. Maintaining adequate low-temperature mechanical properties, including strength, ductility, and toughness, is crucial to assuring structural integrity during low-temperature service. Microscopically, the mechanical properties of metals and alloys at room to cryogenic temperatures are primarily controlled by the formation and migration of extended defects such as stacking faults, dislocations, and twins. In general, defect nucleation and motion are stress-assisted, thermally activated processes. At low temperatures, the reduced intensity of thermal activation not only increases the difficulty of defect activity, but also affects the competition between dislocation glide and deformation twinning as the primary deformation mechanism [1]. Largely as a consequence of diminished defect activity, many metals and alloys that have good room-temperature mechanical properties do not perform adequately at lower temperatures [2–4].

* Corresponding authors.
E-mail addresses: Yu, Q. (yu_qian@zju.edu.cn), Zhu, T. (ting.zhu@me.gatech.edu), Ritchie, R.O. (roritchie@lbl.gov).

 https://doi.org/10.1016/j.mattod.2019.03.001

Single-phase, face-centered cubic (*fcc*) alloys normally maintain ductility as temperature decreases. For example, *fcc* materials such as austenitic stainless steels and aluminum alloys exhibit a mild reduction in ductility at low temperatures, although a few *fcc* materials, such as aluminum-lithium alloys [5], become much tougher with decrease in temperature below ambient. Recently, it has been shown that *fcc* CrCoNi-based medium- to high-entropy alloys can be included in the latter category [6–12]. Notably, the equiatomic alloys CrCoNi and CrMnFeCoNi alloys have been found to display exceptional tensile ductility and fracture toughness at cryogenic temperatures [9,10]. Different from traditional metallic alloys that usually involve one primary element, medium- to high-entropy alloys comprise multiple elements generally with equiatomic compositions [13,14]. A notable high-entropy alloy is the so-called Cantor alloy CrMnFeCoNi [13]. Previous *in situ* transmission electron microscopy (TEM) experiments reported that at room temperature, partial and full dislocations dominate deformation in this alloy [15], while dislocation slip and twinning prevail in the medium-entropy CrCoNi alloy [16]. Such active operation of partial dislocations and twins has been related to the low stacking fault energy (SFE), which has been experimentally determined at room temperature to be approximately 22 $mJ{\cdot}m^{-2}$ for CrCoNi [17] and 30 $mJ{\cdot}m^{-2}$ for CrMnFeCoNi [18], although these numbers may vary with temperature. As temperature decreases, twinning deformation appeared in the CrMnFeCoNi alloy and thus contributes to the strength and ductility at cryogenic temperatures [7]. However, with only *post-mortem* TEM analysis available on the microstructures in these alloys before and after deformation at low temperatures [7,17], the dynamic defect behavior, microstructural evolution, and intrinsic deformation mechanisms during straining remain unclear; such information is essential to enhance our understanding of the fundamental origins of the high strength, ductility, and fracture toughness of these alloys at low temperatures.

In the present study, we investigate the mechanistic origin of the excellent low-temperature strength and ductility of CrCoNi-based medium- and high-entropy alloys by conducting *in situ* TEM deformation experiments at a cryogenic temperature of 93 K (−180 °C). We examine the Cantor high-entropy alloy, CrMnFeCoNi, and two of its derivatives, CrFeCoNiPd and CrCoNi, all of which are single-phase, equiatomic, *fcc* solid solutions. Similar to the better known CrCoNi and CrMnFeCoNi alloys (with uniaxial stress-strain curves respectively given in refs. 9 and 10), the CrFeCoNiPd alloy also exhibits enhanced mechanical properties with decreasing temperature (Fig. S1 in the Supplementary Material). Indeed, the replacement of Mn in the Cantor alloy by Pd changes the SFE and intrinsic lattice resistance for dislocations in the new CrFeCoNiPd alloy, given the apparently large differences in atomic size, mass, and chemical affinity of Pd with the other four elements. Our *in situ* TEM experiments show that the room-temperature deformation of the CrFeCoNiPd alloy involves the motion of full dislocations exclusively (Fig. S2), which indicates higher SFE of the CrFeCoNiPd alloy relative to the other two alloys. Hence, a comparison study of the three CrCoNi-based alloys through cryogenic temperature TEM (cryo-TEM) allows us to assess the impact of SFE on deformation mechanisms at low temperatures. Using real time cryo-TEM imaging of the dynamic deformation defects at the nanoscale, we observed multiple deformation mechanisms, including deformation twinning, glide of partial and full dislocations, extensive cross-slip of screw dislocations, and grain-boundary-initiated multiple slip and twinning at cryogenic temperatures. By comparing the mechanical behavior and associated deformation mechanisms of these three CrCoNi-based alloys at cryogenic and room temperatures, we find that stress and thermal activation can markedly influence their deformation mechanisms and resulting mechanical properties, and that this effect becomes stronger at low temperatures. This is attributed to the reduced thermal energy available for nucleation and migration of deformation-induced defects at lower temperatures.

Material and methods

The medium- to high-entropy alloys of CrCoNi, CrMnFeCoNi, and CrFeCoNiPd tested are all equiatomic *fcc* solid solutions. The CrCoNi and CrMnFeCoNi alloys were from batches of material used in our previous work where details of their processing can be found [9,10]. The CrFeCoNiPd alloy was produced by arc-melting pure Fe, Co, Ni, Cr, and Pd metals (>99.9% purity), with the same method as described previously [7]. To ensure thorough mixing of all elements, the arc-melted buttons were flipped and re-melted five times, followed by drop-casting into a Cu mold with dimensions of $12.7 \times 12.7 \times 70\ mm^3$. The cast bars were homogenized in vacuum at 1200 °C for 24 h before rolling into 1.8-mm sheets at room temperature. Equiaxed grain microstructures with an average grain size of ~130 μm were obtained after recrystallization for 1 h at 1150 °C.

For *in situ* cryo-TEM straining tests, the samples were prepared using a twin-jet electro-polisher in an acetic acid solution containing 10 vol.% perchloric acid at 30 mA and 10 °C. The electron transparent area was placed upon the rectangular hole and the sample was glued on the tension substrate (Fig. 1). We then mounted the tensile sample onto a Gatan single-tilt straining holder with two screws. *In situ* straining experiments were conducted at 93 K (−180 °C) in an FEI Tecnai G^2 F20 TEM operating at 200 kV, with the tensile sample directly cooled by heat transfer of liquid nitrogen from a container at the end of the holder. *Post-mortem* analysis using atomic-resolution high-angle annular dark field scanning transmission electron microscopy (HAADF-STEM) images were conducted on an aberration-corrected scanning transmission electron microscope equipped with a HAADF detector and an ADF detector. The straining tests were conducted in the displacement-control mode.

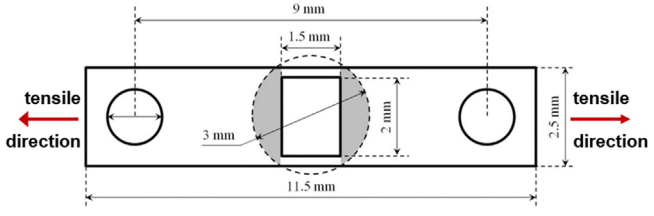

FIGURE 1

Schematic illustration of the specimen geometry for *in situ* TEM tensile tests.

Results and discussion

Deformation twinning

Previous studies [7,15–17] indicated that at room temperature, the deformation of the CrMnFeCoNi alloy involved mainly partial and full dislocations, whereas the corresponding deformation modes of the CrCoNi alloy additionally involved deformation twinning. In contrast, full dislocations dominated the room-temperature deformation behavior of the CrFeCoNiPd alloy with no deformation twinning. At 93 K, the formation of deformation twins was frequently observed in all three alloys (Fig. 2). Most primary twins nucleated directly from grain boundaries, while secondary twins emanated from the boundaries between primary twins and the matrix. Fig. 3 reveals the dynamic process of deformation twinning at 93 K, with the CrFeCoNiPd alloy as an example. Fig. 3a shows the emission of an array of partial dislocations from the grain boundary to form nano-twins; the associated

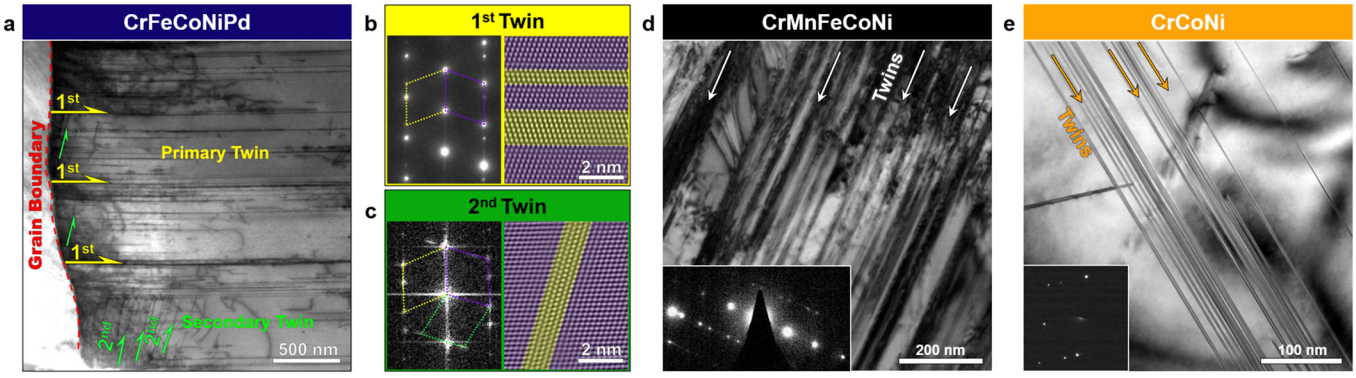

FIGURE 2

Twins formed during *in situ* tensile straining tests at 93 K. (a) Low magnification bright-field (BF) STEM image of the nano-twins. (b) Diffraction patterns (left) and high-resolution HAADF images (right) are shown for primary twins. (c) Fast Fourier transform (FFT) image of primary and secondary twins (left) and high-resolution HAADF images (right) of secondary twins. (d–e) Low magnification BF-STEM images of the nano-twins in CrMnFeCoNi and CrCoNi alloys, respectively. Insets show the selected area electron diffraction patterns of the twins.

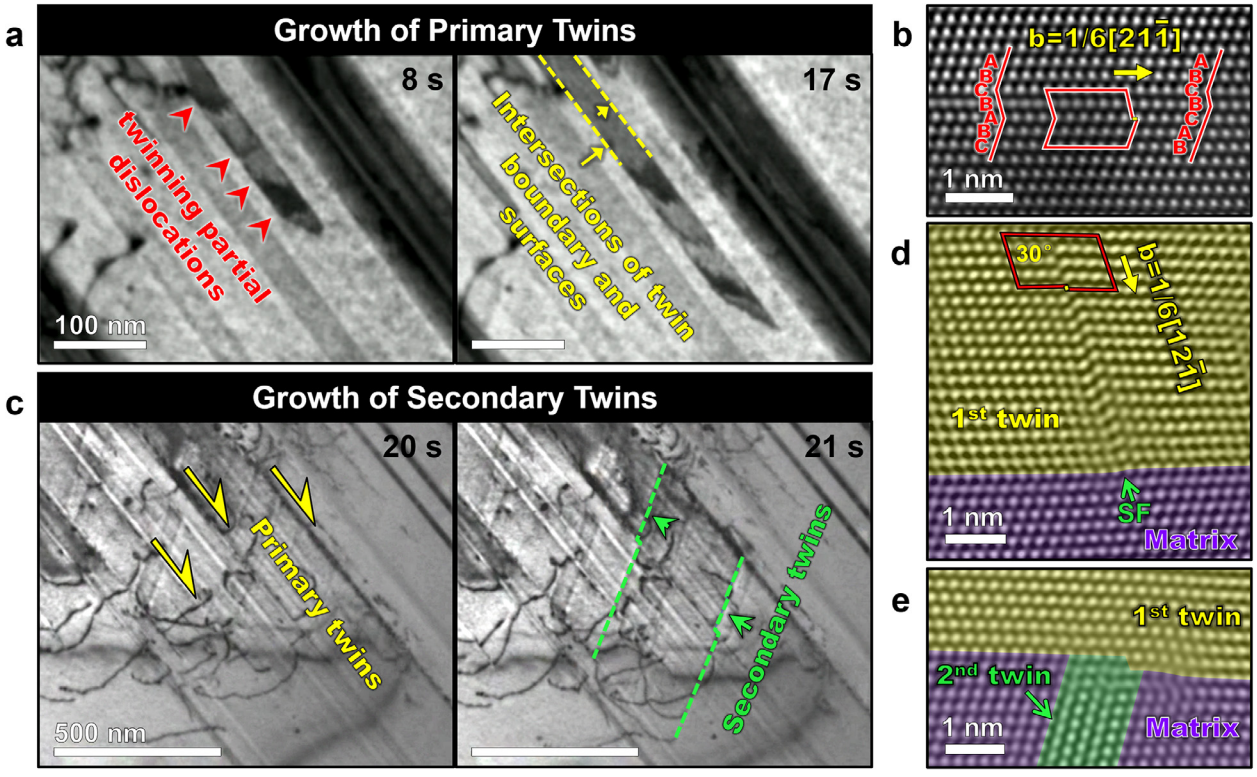

FIGURE 3

Twinning deformation in the CrFeCoNiPd alloy at 93 K. (a) TEM screenshots from Supplementary Video 1 showing the process of formation of a primary twin. An array of twinning partial dislocations was emitted from a grain boundary. Boundaries marked by yellow dashed lines are at intersections between the upper and lower surfaces of the TEM sample and the nascent twin. (b) Filtered atomic-resolution HAADF STEM image of a growing twin with viewing direction along ⟨110⟩. (c) TEM screenshots from Supplementary Video 2 showing the initial stage of the nucleation of secondary twins, as twinning partial dislocations were emitted from the primary twin boundaries. (d) Atomic structure of a partial dislocation emitted from a primary twin boundary. (e) Filtered high-resolution HAADF-STEM image showing the atomic structure of the intersection between the primary and secondary twins.

real-time processes are shown in Supplementary Video 1. Detailed analysis of Fig. 3a indicates that both the forward propagation of the twin tip and the lateral migration of the twin boundaries occurred by glide of 1/6 {1 1 1} ⟨112⟩ twin partial dislocations. Fig. 3b shows the atomic structure of twin partials at a growing twin tip viewed end-on (along the out-of-plane beam direction of ⟨110⟩). From the filtered high-resolution HAADF-STEM image, the Burgers vector of the twin partials was determined to be $1/6\left[2\,1\,\bar{1}\right]$. With increasing applied strain, partial dislocations emitted from the boundaries of primary twins were seen to glide on conjugate {1 1 1} slip planes, forming secondary twins (as shown in Fig. 3c and Supplementary Video 2). The atomic-resolution HAADF image in Fig. 3d also shows the emission of a $1/6\left[1\,2\,\bar{1}\right]$ partial dislocation from the boundary of a primary twin. Successive emission of such partial dislocations on consecutive {1 1 1} planes resulted in the formation of a secondary twin (Fig. 2c and Fig. 3e). The formation of the primary and secondary nano-twins effectively sub-divided the initial coarse grains (~130 μm in size) into smaller sub-grains. The twin boundaries were observed to impede dislocation glide on the slip planes inclined to twin boundaries. Such impediments can produce substantial strengthening and increase the strain hardening capability of alloys, as shown in other nano-twinned materials [19–24]. Importantly, similar formation and growth processes of the primary and secondary twins were observed in the CrMnFeCoNi and CrCoNi alloys as well (Fig. 2d-e), indicating that twinning serves as an important deformation mechanism in all three alloys at cryogenic temperatures. In contrast, at room temperature, deformation twinning was rarely observed during *in situ* TEM straining in CrMnFeCoNi [15] and CrFeCoNiPd, but often seen in the higher strength CrCoNi alloy with lower SFE [16].

Full dislocations

In addition to the above-mentioned twin partial dislocations that were associated with deformation twinning, full dislocations were active in all three alloys at cryogenic temperatures. Interestingly, we observed a common mode of dislocation glide similar to that observed previously in the CrCoNi alloy at room temperature [16]. Specifically, the coherent twin boundaries, which serve as strong barriers to dislocations that impinge on them, provide long and smooth pathways that promote the glide of the full dislocations at low temperatures, as shown in Fig. 4a, Fig. 5a-b and Supplementary Video 3. In contrast to individual twin partials, motion of these full dislocations generated plastic strains without causing twin boundary migration. As such, twin boundaries play dual roles in acting as both barriers to obstruct the motion of impinging dislocations and pathways to facilitate the glide of dislocations on twin boundaries. Hence, twin boundaries simultaneously contribute to the high strength and ductility in CrCoNi-based medium- and high-entropy alloys at cryogenic temperatures.

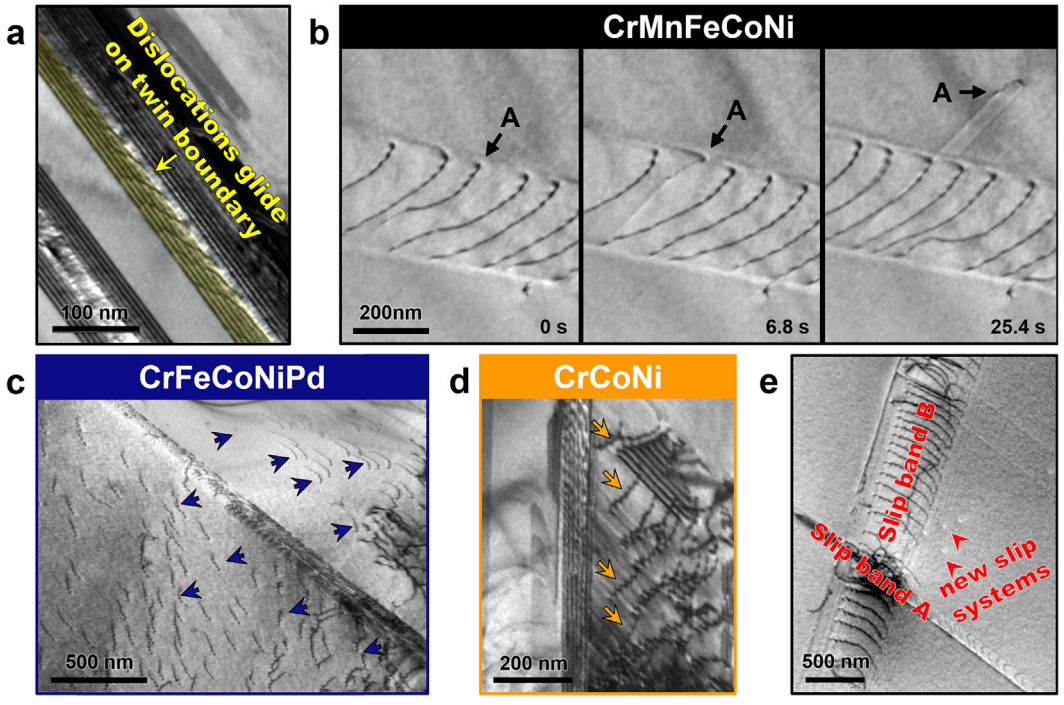

FIGURE 4

Dislocation behavior in CrCoNi-based alloys at 93 K. (a) Screenshot from Supplementary Video 3 showing the motion of full dislocations (split into leading and trailing Shockley partials) on twin boundaries in CrFeCoNiPd. (b) Serial TEM images from Supplementary Video 4 showing a cross-slip process in CrMnFeCoNi. "Dislocation A" cross-slips onto a secondary slip plane when its motion becomes impeded in the primary slip plane. (c–d) Extensive cross-slip processes in CrFeCoNiPd and CrCoNi with individual cross-slip events respectively marked by blue and orange arrows. Further details are shown in Supplementary Videos 5 and 6. (e) Interaction between different slip systems in CrFeCoNiPd (Supplementary Video 7). At the intersection of slip bands A and B, new slip systems are activated, shown by red arrows. Note that the cross-slipped dislocations are generally parallel to the viewing direction, such that the images of the dislocations are end-on.

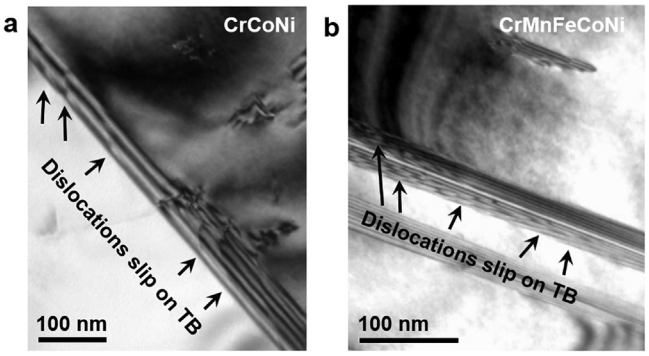

FIGURE 5

Glide of full dislocations on twin boundaries at 93 K in (a) CrCoNi alloy, and (b) CrMnFeCoNi alloy.

Interestingly, we found massive cross-slip of full screw dislocations at the beginning of plastic deformation in all three alloys at cryogenic temperatures. This has not been reported as a major deformation mode in high-entropy alloys previously. The time series of TEM images in Fig. 4b shows a typical cross-slip process of screw dislocations in the CrMnFeCoNi alloy during an *in situ* TEM experiment at 93 K. In this series, one of the screw dislocation lines, labeled as "A", initially glided within a planar {1 1 1} slip band containing a full dislocation pile-up array. As dislocation "A" gradually came to a standstill, part of the dislocation line cross-slipped onto a secondary {1 1 1} slip plane while the rest of the dislocation line remained on the original slip plane. With increasing applied strain, the whole dislocation "A" proceeded to complete the cross-slip and subsequently glided on the secondary {1 1 1} slip plane. Such cross-slip events occurred frequently at different locations within this particular planar slip band (Supplementary Video 4). Fig. 4c-d shows similar events that frequently were observed in the other two CrCoNi-based alloys at 93 K (see Supplementary Videos 5 and 6). Double cross-slip also occurred, such that the cross-slipped dislocations in the secondary slip plane returned to the original slip plane. Eventually, a high density of cross-slip events resulted in a homogeneous distribution of dislocations (Fig. 4c-d). Without *in situ* cryo-TEM observation, the origin of intense dislocation activities at cryogenic temperatures may not be associated with massive cross-slip since it was thought to be unlikely before. Also, one could not clearly determine the sources of dislocations in different slip systems from *post-mortem* TEM analysis. These extensive cross-slip activities facilitated the strong interactions among dislocations in the primary and secondary slip systems. One example is shown in Fig. 4e and Supplementary Video 7, where significant dislocation interactions were observed at the intersection of the two slip systems at which local stress concentrations led to activation of a new slip system. Such a high frequency and density of cross-slip events resulted in homogeneously distributed micro-slip inside the grains and also promoted strain hardening during the early stage of plastic deformation [25]. These effects are deemed to contribute to the superior mechanical properties of these medium- and high-entropy alloys at cryogenic temperatures.

The extensive cross-slip activities and subsequent dislocation multiplication and interactions can be reasonably related to the high operating stresses during plastic deformation of the CrCoNi-based medium- and high-entropy alloys at low temperatures. On the one hand, thermal activation of defects becomes more difficult with decreasing temperature, such that the applied stress has to be elevated to activate defects at sufficient frequencies for continued plastic flow. On the other hand, the multicomponent atomic structures of concentrated solid solutions can exhibit many local chemical structure fluctuations, which result in local secondary barriers to dislocation motion [26–28], in addition to primary barriers such as the short-range pinning obstacles of forest junctions and the long-range internal stresses induced by heterogeneous grain and dislocation microstructures. These secondary barriers can be sufficiently strong to increase the effective frictional resistance to dislocation motion [28]. In addition, the strong secondary barrier can act to locally constrict the stacking fault between the leading and trailing partials of the screw dislocation. Such local constriction, together with the elevated applied stress, promotes cross-slip. As discussed earlier, during plastic deformation at room temperature, the three alloys of CrFeCoNiPd, CrMnFeCoNi, and CrCoNi were found to display markedly different levels of activity of the partial dislocations and twins. This is in accord with the different SFEs of the three alloys [17,18,29], which is also consistent with the fact that extensive cross-slip was only observed in the CrFeCoNiPd alloy at room temperature. In contrast, the active operation of cross-slip in all three alloys at cryogenic temperatures indicates that the SFE, which determines the equilibrium stacking fault width in the core of the extended dislocation, becomes less important in dictating cross-slip.

Dislocation-grain boundary interactions

In addition to intragranular deformation mechanisms, we also investigated the role of grain boundaries in plastic deformation at cryogenic temperatures. Grain boundaries are in general considered as a potent source of strengthening as they impede dislocation motion; on the other hand, ductility can be adversely affected by grain boundaries, since deformation incompatibilities between adjoining grains can lead to damage and fracture at grain boundaries [2]. Here we find that at low temperatures, grain boundaries can promote multiple slip and deformation twinning within adjacent grains as well as in the original grain. This was observed in all three alloys but was most prominent in the CrFeCoNiPd alloy. It indicates that grain boundaries remain capable of intense dislocation interactions at cryogenic temperature. An example is shown in the series of TEM images in Fig. 6a, taken from Supplementary Video 8. An array of dislocations in slip band E (marked by red arrow) inside grain 1 approached the grain boundary and then stopped. The interactions between this array of impinging dislocations and the grain boundary gradually activated four new slip systems, yielding about ten individual slip bands (as indicated by green, blue, orange and yellow arrows in Fig. 6a) in the two adjoining grains at the grain boundary. In addition, we also observed partials and nano-twins emitting from the same grain boundary (Fig. 6b). In concert with intragranular deformation mechanisms, the active operation of multiple deformation mechanisms at grain boundaries is deemed to effectively enhance strength and ductility.

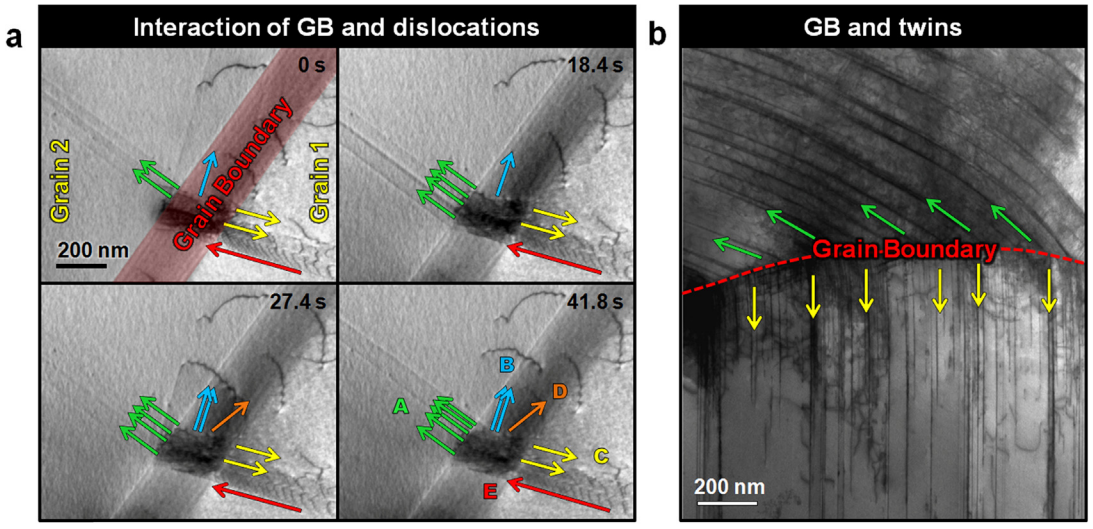

FIGURE 6

Interactions between grain boundaries and dislocations in the CrFeCoNiPd alloy at 93 K. (a) Series of TEM images from Supplementary Video 8 showing the activation of multiple slip systems at a grain boundary. Four slip systems (marked as A, B, C and D) with about ten glide bands (indicated by green, blue, orange, and yellow arrows) are activated when an array of dislocations (indicated by red arrow E) interacts with the grain boundary. (b) A high density of nano-twins is formed in the adjoining grains since the grain boundary emits partials into both grains.

Theoretical analysis

To provide some theoretical basis to further understand the impact of temperature on deformation mechanisms, we note that in general, the activation of a specific type of extended defect, such as partial dislocations, full dislocations and twins, is controlled by both mechanical stresses and thermal fluctuations. The applied stress determines the thermal activation energy, varying from zero at the so-called athermal limit to a maximum which represents the energy barrier when the applied stress is zero. According to transition state theory, to achieve a reasonable frequency (*e.g.*, 1/s) for the nucleation and migration of a defect, the stress-dependent activation energy should be no more than 25 k_BT (where k_B is the Boltzmann constant and T is the temperature in Kelvin) [30], which at room temperature (300 K) is about 0.62 eV and at a cryogenic temperature of 93 K is about 0.2 eV. Because of the reduced intensity of thermal fluctuations at 93 K, the applied stress has to be elevated to lower the activation energy to the order of 0.2 eV. As schematically illustrated in Fig. 7, when the applied stress increases, the activation energies for partial dislocations, full dislocations and twins are all reduced, such that their differences become much smaller. As a result, the frequency of nucleation and migration becomes closer for different types of extended defects. Accordingly, we attribute the concurrent operation of multiple defect mechanisms at cryogenic temperatures to the increasing impact of stress activation and the concomitantly reduced influence of thermal activation. Moreover, the increase of the applied stress with decreasing temperature is manifested in terms of a higher density of defects, such as twins. It follows that a multitude of stress-driven extended defects can collectively facilitate the extensive plastic deformation and promote the strain hardening, thereby leading to the outstanding mechanical properties of medium- and high-entropy alloys at low temperatures.

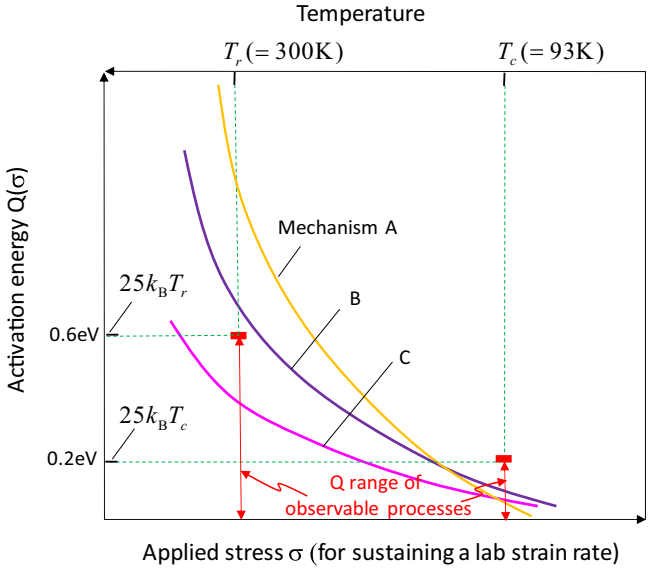

FIGURE 7

Schematic illustration showing that at low temperatures and high stresses, different defect processes in medium- to high-entropy alloys could all be activated. Mechanisms A, B, C can be considered as twinning, cross-slip, and dislocation glide, respectively. For alloys with different stacking fault energies, both the relative magnitudes and cross-over points of the activation energy curves may vary. To sustain an applied strain rate in a typical laboratory experiment, the frequency v of thermal activation of defect processes, such as dislocation de-pinning from obstacles, screw cross-slip, twin nucleation, should be on the order of 1/s. From transition state theory, v is given by $v = v_0 \exp[-Q(\sigma)/k_BT]$, where $Q(\sigma)$ is the activation energy that depends on the applied stress σ, k_B is Boltzmann's constant, and T the absolute temperature. Given a typical trial frequency v_0 of 10^{11} s^{-1}, $Q(\sigma)$ needs to be no more than 25 k_BT, which corresponds to ~0.6 eV at room temperature (T_r = 300 K) and ~0.2 eV at cryogenic temperature (T_c = 93 K), respectively. To lower the activation energies, one would have to increase the applied stress.

Conclusions

We have performed *in situ* TEM straining experiments at cryogenic temperatures (~93 K) to study the mechanistic underpinnings of the excellent combinations of strength and ductility of CrCoNi-based medium- and high-entropy alloys at low temperatures. Extending the initial explanations for the exceptional damage tolerance of these alloys at low temperatures, which were principally attributed to deformation twinning [9,10], we now show that a synergy of plastic deformation mechanisms is active in addition to twinning, including the glide of partials and full dislocations, extensive cross-slip, and multiple slip activated by dislocation and grain-boundary interactions, all of which can concurrently operate in the CrMnFeCoNi, CrFeCoNiPd and CrCoNi alloys at cryogenic temperatures. These extended defects are highly active and strongly interact with each other, collectively enabling the remarkable high strength and ductility of these single-phase, medium- and high-entropy alloys at low temperatures. In contrast, the room-temperature deformation mechanisms in the three alloys involve markedly different activities of partial dislocations and twins. This is partly related to their different SFEs, and more importantly to the different primary extended defects that control the mechanical properties of these alloys at room temperature.

Finally, we note the formidable role that cryogenic-temperature TEM experiments can play in the nanoscale understanding of the mechanistic basis for structural performance. For example, without *in situ* cryo-TEM observations, the origin of intense dislocation activities may not be realized as massive cross-slip, particularly as it was thought to be unlikely before. Thus, cross-slip would probably not be linked to the homogeneously distributed micro-slips as well as the hardening responses during the early stage of plastic deformation in the three alloys studied. *In situ* cryo-TEM can therefore not only provide critical insights into the understanding of the deformation mechanisms underpinning the mechanical behavior of the present CrCoNi-based medium- to high-entropy alloys, but can also be extended for other studies of advanced metals and alloys at low homologous temperatures.

Data availability

Data associated with the transmission electron microscopy are available from Prof. Qian Yu at Zhejiang University (email: yu_qian@zju.edu.cn).

Acknowledgments

QY was supported by the Chinese 1000-Youth-Talent Plan, 111 project under Grant No. B16042, National Natural Science Foundation of China (51671168) and the State Key Program for Basic Research in China under Grant No. 2015CB65930. TZ was supported by the U.S. National Science Foundation under grant no. DMR-1810720. HB and EPG were supported by the U.S. Department of Energy, Office of Science, Basic Energy Sciences, Materials Sciences and Engineering Division. BG and ROR were supported by the U.S. Department of Energy, Office of Science, Office of Basic Energy Sciences, Materials Sciences and Engineering Division and under contract no. DE-AC02-05CH11231 to the Mechanical Behavior of Materials Program (KC13) at the Lawrence Berkeley National Laboratory (LBNL).

Appendix A. Supplementary data

Supplementary data to this article can be found online at https://doi.org/10.1016/j.mattod.2019.03.001.

References

[1] A.S. Argon, Strengthening Mechanisms in Crystal Plasticity, Oxford Unversity Press, New York, 2008.
[2] A.H. Cottrell, Trans. Am. Inst. Mining Metall. Eng. 212 (1958) 192.
[3] R.W. Armstrong, Acta Metall. 16 (1968) 347.
[4] A.S. Argon, J. Eng. Mater. Technol. 123 (2001) 1.
[5] K.T.V. Rao, W. Yu, R.O. Ritchie, Metall. Trans. A 20 (1989) 485.
[6] A. Gali, E.P. George, Intermetallics 39 (2013) 74.
[7] F. Otto et al., Acta Mater. 61 (2013) 5743.
[8] Z. Wu et al., Acta Mater. 81 (2014) 428.
[9] B. Gludovatz et al., Science 345 (2014) 1153.
[10] B. Gludovatz et al., Nat. Commun. 7 (2016) 10602.
[11] A.J. Zaddach, R.O. Scattergood, C.C. Koch, Mater. Sci. Eng., A 636 (2015) 373.
[12] Y.H. Jo et al., Nat. Commun. 8 (2017) 15719.
[13] B. Cantor et al., Mater. Sci. Eng., A 375 (2004) 213.
[14] J.W. Yeh et al., Adv. Eng. Mater. 6 (2004) 299.
[15] Z. Zhang et al., Nat. Commun. 6 (2015) 10143.
[16] Z. Zhang et al., Nat. Commun. 8 (2017) 14390.
[17] G. Laplanche et al., Acta Mater. 128 (2017) 292.
[18] N.L. Okamoto et al., Sci. Rep. 6 (2016) 35863.
[19] J.W. Christian, S. Mahajan, Prog. Mater Sci. 39 (1995) 1.
[20] K. Lu, L. Lu, S. Suresh, Science 324 (2009) 349.
[21] Y.B. Wang et al., Mater. Sci. Eng., A 527 (2010) 4959.
[22] S. Ni et al., Acta Mater. 60 (2012) 3181.
[23] Y.T. Zhu, X.Z. Liao, X.L. Wu, Prog. Mater Sci. 57 (2012) 1.
[24] Y. Wei et al., Nat. Commun. 5 (2014) 3580.
[25] F.R.N. Nabarro, Acta Metall. 37 (1989) 1521.
[26] C. Varvenne, A. Luque, W.A. Curtin, Acta Mater. 118 (2016) 164.
[27] F.X. Zhang et al., Phys. Rev. Lett. 118 (2017) 205501.
[28] S. Saroukhani, D.H. Warner, Acta Mater. 128 (2017) 77.
[29] S. Zhao, G.M. Stocks, Y. Zhang, Acta Mater. 134 (2017) 334.
[30] A.H. Cottrell, Phil. Mag. 86 (2006) 3811.